Fractional-Order Stochastic Extremum Seeking Control with Dithering Noise for Plasma Impedance Matching

Jairo Viola[1], Derek Hollenbeck[1], Carlos Rodriguez[1,2], and YangQuan Chen[1]

***Abstract*— Impedance matching is critical to ensure the maximum power transfer on plasma etching for semiconductor manufacturing. However, it is a challenging task due to the unknown and complex plasma dynamics. In this paper, a Stochastic Perturb and Observe Fractional-Order Extremum Seeking Controller (P&O FO-SESC) is employed for plasma impedance matching. The controller uses a Fractional-Order Gaussian (dithering) Noise (fGn) as the perturbation signal and is tested for an L-type matching network with two variable capacitors. Obtained results show that the Stochastic P&O FO-ESC controller improves the impedance matching convergence zone over the standard P&O ESC controller for different loads and initial conditions.**

I. Introduction

Plasma etching is a widely used technique in semiconductor manufacturing, which employs a Radio Frequency (RF) power supply to drive and stabilize a plasma load. It uses an impedance matching network that matches the generator output impedance with the plasma load to ensure the maximum power transfer from the RF source. However, the impedance matching is a challenging task due to the plasma's unknown and complex dynamic. There are different control approaches to perform automatic plasma impedance matching [1]–[4], which employ seeking algorithms based on the magnitude and phase of the combined impedance of the matching network and plasma load. In these applications, the reflected power or other performance indices are not considered, and requires a feedforward setup to ensure the impedance matching. Likewise, the proposed control schemes are evaluated only for one specific load without exploring the complete matching space of the network as well as different pairs of capacitor initial conditions. Thus, the convergence and robustness analysis of these techniques are limited and cannot be generalized.

Besides, Extremum Seeking Control (ESC) is an adaptive model free technique that allows optimizing smooth convex function problems, which extremum may be unknown and variable [5]–[7]. For the impedance matching problem, [5] shows its application into an L-Type matching network, using Sliding Mode and Perturb and Observe ESC controllers. This approach is extended into Fractional-Order ESC by [1], [8], where the Fractional-Order Sliding Mode Extremum Seeking Control is proposed for a class of nonlinear systems including the impedance matching for single capacitor L-Type network. Likewise, a Fractional-order version of the stochastic perturb and observe ESC controller introduced by Liu in [9] is presented by [10]. In this case, the perturbation signal is replaced by a bounded fractional-order dithering Random Noise (Gaussian (fGn) or Symmetric Alpha-Stable (SαS)) with Long-Range Dependence (LRD) determined by the noise Hurst Exponent.

This paper presents the use of Stochastic perturb and observe FO-ESC controller (P&O FO-SESC) for the impedance matching problem with multiple actuators. The matching network is an L-Type with two variable capacitors using the reflected power as optimization variable. The P&O FO-SESC controller is employed to perform the impedance matching and is compared with the perturb and observe sinusoidal ESC controller (P&O ESC) for different plasma loads and capacitors initial conditions (IC).

The main contribution of this paper is the use of Stochastic Perturb and Observe ESC controllers (P&O FO-SESC) with dithering noise for plasma impedance matching with multiple actuators and its performance assessment under different plasma loads, capacitor IC, and noise levels given by the values of the Hurst exponent.

II. Extremum Seeking Control

There are several formulations for ESC controllers such as perturb and observe [6], sliding mode [11], or relay based [12]. In this paper, the sinusoidal P&O ESC and P&O FO-SESC controllers are employed for the impedance matching problem.

A. Sinusoidal Perturb and Observe ESC Controller

The structure of the sinusoidal perturb and observe ESC controller is shown in Fig. 1 [6]. Initially, a sinusoidal perturbation signal with amplitude a and frequency w is added to the estimated optimal parameter $\hat{\theta}$. Then, it is applied to the plant by the actuator $U(\theta)$ producing a new value of the cost function $f(\theta)$ (1), where f^* is the optimal value of f produced by the optimal parameter θ^*. Thus, the produced system output y (2) is passed through a high-pass filter with pole h, acting like a function gradient multiplied by the perturbation signal producing $\eta = \dot{\theta}$ that is then integrated, producing a new $\hat{\theta}$ with error dynamics $\dot{\tilde{\theta}}$ stable for $k, a, f" > 0$ as demonstrated by [6] where k is the integrator gain and a the disturbance scaling factor. As a condition for the ESC controller stability, $f"$ must exist and f should be a smooth function.

[1]Jairo Viola, Derek Hollenbeck, and YangQuan Chen are with School of Engineering, University of California Merced, CA 95340 USA {jviola,dhollenbeck,ychen53}@ucmerced.edu
[2]Carlos Rodriguez is with Ensenada Center for Scientific Research and Higher Education, Mexico {crodriguez}@cicese.edu.mx

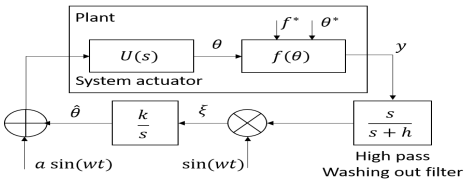

Fig. 1. Sinusoidal P&O ESC controller [6]

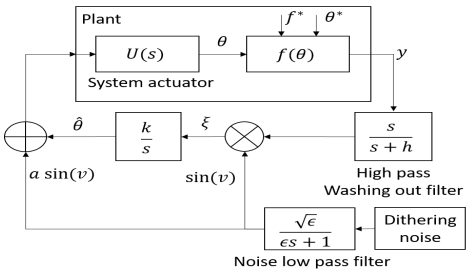

Fig. 2. Fractional-Order P&O SESC controller [9]

$$f(\theta) = f^* + \frac{f"}{2}(\theta^* - \theta)^2 \tag{1}$$

$$y = f^* + \frac{a^2 f"}{4} + \frac{f"}{2}\tilde{\theta}^2 - af"\tilde{\theta}\sin(wt) + \frac{a^2 f"}{4}cos(2wt) \tag{2}$$

$$\dot{\tilde{\theta}} = -\frac{ka^2 f"}{4}\tilde{\theta} \tag{3}$$

B. Stochastic Fractional-Order Perturb and Observe ESC Controller

The P&O FO-SESC controller is shown in Fig. 2. It is based on the stochastic ESC control introduced by [9] which structure is similar to the P&O IO-ESC controller. The main difference is that the perturbation signal ν corresponds to a bounded stochastic dithering noise that can be Integer-Order Gaussian (Brownian motion), Symmetric Alpha Stable SαS, or Fractional-order Gaussian (fGN). The disturbance signal is passed through a low pass filter to cut-off the high frequency components of the random noise to perform a better optimum seeking.

In the case of fractional Gaussian noise, it can be represented as the change in Brownian motion steps, which is defined using the Riemann-Liouville fractional integral as shown by (4), where $dB(s)$ is the general definition of white noise, $\Gamma(\cdot)$ is the gamma function, and H is the Hurst exponent which indicates the LRD property of the random disturbance signal [13], [14]. According to the value of H, the dithering noise time series can represent a Brownian motion if $H = 0.5$, positively correlated if $0.5 < H < 1$ and negatively correlated if $0 < H < 0.5$. In this case, the dithering noise is considered fractional-order Brownian motion if $H \neq 0.5$. The exponential stability of the P&O FO-SESC controller is demonstrated in [9] for $f"(\hat{\theta}) > 0$ and $ka > 0$.

$$B_H(t) = \frac{1}{\Gamma(H+1/2)}\int_0^t (t-s)^{H-0.5}dB(s). \tag{4}$$

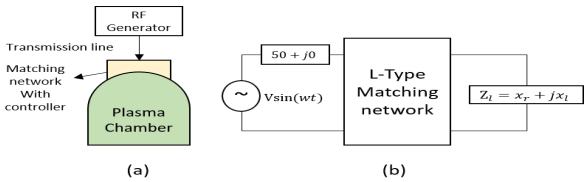

Fig. 3. Impedance matching a) process diagram and b)schematic representation

III. Plasma Impedance Matching

The setup for a plasma impedance matching problem is shown in Fig. 3a. As can be observed, the RF source send the power to the chamber where the plasma is contained, and using the matching network at the input of the chamber, the maximum power transfer between the plasma and the RF source is ensured. Its schematic representation is shown in Fig. 3b for a $50 + j0\Omega$ generator output impedance. In this case, the power in the load P_l can be calculated as the difference between the forward P_f and reflected power P_r as is given by

$$P_l = \frac{1}{2}V_s\frac{R_l}{Z_s + Z_l}\frac{V_s}{(Z_s + Z_l)^*}, \tag{5}$$

where V_s is the source voltage, Z_l is the load impedance, Z_s is the generator output impedance, and $(Z_s + Z_l)^*$ the complex conjugate of $Z_s + Z_l$. Likewise, the maximum power transfer is reached when $Z_s = Z_l^*$, which can be quantified using the reflection coefficient index Γ for the load that is bounded from zero to one, with zero indicating no reflected power.

$$\Gamma = \frac{Z_l - Z_s}{Z_l + Z_s}. \tag{6}$$

A. L-Type impedance matching network

The impedance matching network employed corresponds to an L-type shown in Fig. 4. It is composed by a shunt C_t and series C_m variable capacitors actuated by a stepped motor. The shunt and series capacitors comes with a shunt and series inductance L_t and L_m respectively. The total impedance Z_{in} view from the generator output is calculated as follows. Initially, the impedance sum of series branch Z_m with the load Z_l is given by (7). The shunt branch impedance Z_t is given by (8). Thus the total impedance Z_{in} is the parallel of Z_m and Z_t as shown by (9).

$$Z_m + Z_l = R_0 + j(wL_m - \frac{1}{wC_m} + X_0), \tag{7}$$

$$Z_t = jwL_t + \frac{1}{jwC_t}, \tag{8}$$

$$Z_{in} = \frac{Z_t(Z_m + Z_l)}{Z_t + Z_m + Z_l}. \tag{9}$$

The parameters for the L-Type network employed in this paper are a generator output impedance $Z_s = 50 + j0$, $425pF \leq C_t \leq 2240pF$, $114pF \leq C_m \leq 445pF$, $L_t =$

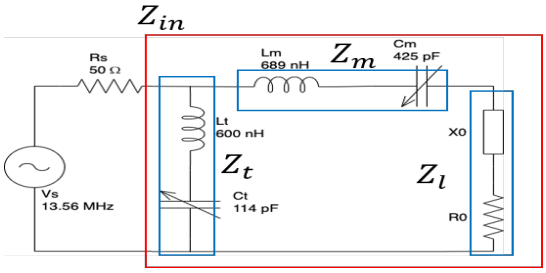

Fig. 4. L-Type Impedance matching network

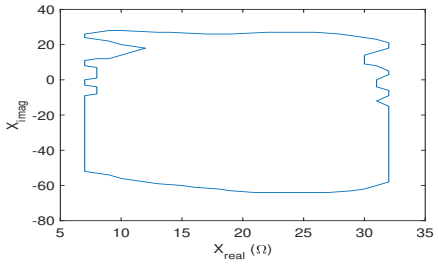

Fig. 5. Feasible matching region for L-Type network

$600nH$, $L_m = 689nH$, and an RF source frequency of 13.56 MHz. The matching space for the L-type network is shown in Fig. 5. As can be observed, under the current configuration, the matching network match for loads $Z_l = X_{real} + jX_{imag}\Omega$ with real and complex parts between $7 < X_{real} < 32\ \Omega$ and $-60 < X_{imag} < 30\ \Omega$ respectively.

On the other hand, the capacitor space is the relation between the capacitor position and the reflected power coefficient. It is worth to be analyzed considering that the ESC minimizes the reflected power using C_t and C_m as control inputs, which varies from load to load. As example, Fig. 6 shows the capacitor space for the load $Z_l = 7.95 + j5.2\Omega$ with an optimal matching point around $C_t = 550pF$ and $C_m = 180pF$. Notice that there are flat regions that represent a controllability challenge for the ESC controllers due to the fact that its gradient can be vanished quickly. For this reason, it is important to analyze the impedance matching problem not only for a single load and capacitor initial conditions but for the whole feasible matching region and capacitor space.

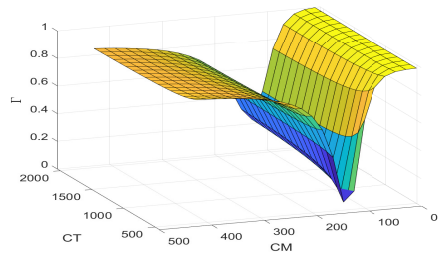

Fig. 6. Capacitor-space (starting capacitor positions) for L-Type network for given $Z_l = 7.95 + j5.2\Omega$

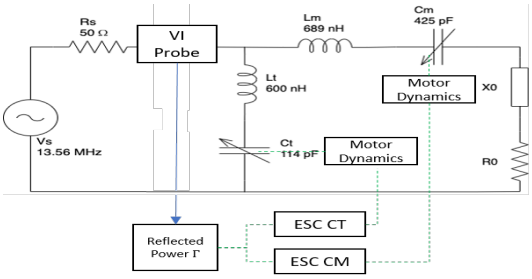

Fig. 7. MIMO ESC Controller with L-Type matching network

TABLE I
P&O ESC AND P&O FO-SESC CONTROLLER PARAMETERS

Parameter	P&O ESC Controller		FO-SESC Controller	
	C_m	C_t	C_m	C_t
High pass filter pole (h)	2π	2π	2π	2π
Integrator gain (k)	100	3000	300	100
Amplitude correction (a)	1.5	2	0.1	0.1
Sinusoidal disturbance frequency (rad/s)	10	7	-	-
Noise mean (μ)	-	-	0	0
Noise Std (σ)	-	-	0.2	0.3
Noise signal amplitude	1	1	150	70
Low-pass noise filter pole ($epsilon$)	-	-	1	1
Hurst exponent (H)	0.1:0.1:0.9			

IV. ESC Controllers Design

The ESC control architecture for the impedance matching network is shown in Fig. 7. It employs two independent ESC controllers, one for the shunt and series capacitors C_t and C_m respectively. The motor response should be included on the system model considering that the electrical dynamic response of the system is much faster compared with the motor dynamics of the variable capacitors. It is described by a second-order transfer function with 20ms settling time given by (10).

$$U(s) = \frac{1}{0.0004s^2 + 0.04s + 1}. \tag{10}$$

The cost function employed for the P&O ESC and P&O FO-SESC controllers is the reflected power of the impedance matching network that is defined by (6). In a real L-type network, the input impedance Z_{in} is measured by a Voltage-Current (VI) probe as shown in Fig. 7. In this paper, Z_{in} is calculated using (9) according to the values of C_t and C_m. The tuning parameters employed for the the P&O ESC and P&O FO-SESC controllers are shown in Table I. In the case of P&O ESC controller, the parameters are selected to ensure the correct extremum tracking. Besides, the P&O FO-SESC controller parameters include a zero mean and a small standard deviation dithering noise for C_t and C_m ES controllers. The correction gains and perturbation signal amplitudes are selected bigger for C_m due to its capacitor range. The dithering noise low-pass filter noise is set to 1 and the Hurst exponent values range is 0.1 to 0.9.

V. Simulation Results and Discussions

Three tests are performed to evaluate the P&O-ESC and P&O FO-SESC controllers. In the first test, both controllers perform the impedance matching for a power setpoint of 1500W with a fixed load of $10-j10\Omega$ under multiple initial conditions of C_t and C_m and Hurst exponents in the range $H = 0.1 : 0.1 : 0.9$ to analyze the influence of anti-persistant and LRD behaviors on the SESC searching. The second test evaluates the P&O FO-SESC performance for the total load matching space given by Fig. 5 with $H = 0.1 : 0.1 : 0.9$ under different capacitor IC's. Finally, the third test evaluate the robustness of the P&O FO-SESC and P&O ESC controllers analyzing its convergence the overall capacitor initial conditions space given by Fig. 6 and the loads in the matching space given by Fig. 5.

A. Test 1: P&O ESC and FO-SESC Controllers Time Responses for A Single Given Load Impedance

The time response of the P&O ESC and the P&O FO-SESC controllers is shown in Fig. 8 for the load $10-j10\Omega$ with capacitor initial conditions at $IC = [0, 0]$. It can be observed that the P&O FO-SESC controller reaches the steady state response, with a smooth control effort given by C_t and C_m for either $H = 0.5$ and $H = 0.6$. On the other hand, the sinusoidal P&O ESC controller, is not able to converge, reaching a minimum reflected power coefficient of 0.2. Considering the influence of the capacitor initial conditions on the search, the test is repeated now for $IC = [50, 50]$ and its results are shown in Fig. 9. It can be appreciated that under the new initial conditions, the sinusoidal P&O ESC controller now is able to converge, as well as the P&O FO-SESC controller. The control action for the P&O ESC controller exhibits a more oscillatory behavior compared with the P&O FO-SESC controller.

A repeatability test of the P&O FO-SESC controller is performed in order to analyze its stochastic behavior and the effects of the Hurst exponent over the controller convergence under multiple capacitor IC's. The controllers settling time, the Root Mean Squares value (RMS) of the reflected power coefficient, and the number of convergences of the FO-SESC controller are used as the performance indices. The Hurst exponent of the dithering noise changes in the range $H = 0.1 : 0.1 : 0.9$, and the FO-SESC controller is evaluated 20 times for each value of H. In this case, the ESC controllers are considered to converge if the reflection coefficient $\Gamma \leq 0.04$. The test is performed by 200 seconds and five initial conditions are evaluated $IC = [0, 0], [10, 20], [35, 40], [50, 50], [100, 100]$. Simulation results shows that the P&O ESC controller convergence rate is 100% only for IC=[35,40],[50,50] and zero for the other IC's. Likewise, the P&O FO-SESC have a convergence range between 20% to 60% for all the evaluated capacitors IC's.

On the other hand, Fig. 10 shows the evolution of the average Gamma RMS, convergence events, and settling time for the FO-SESC controller. As can be observed in Fig. 10b, for $H = 0.6$, the reflected power RMS is lower for most of the IC's. Likewise, Fig. 10a and Fig. 10c show that

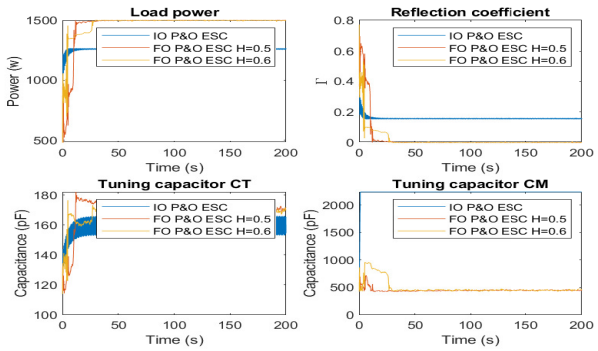

Fig. 8. P&O ESC and P&O FO-SESC controller with load $10-10j$ and IC=[0,0]

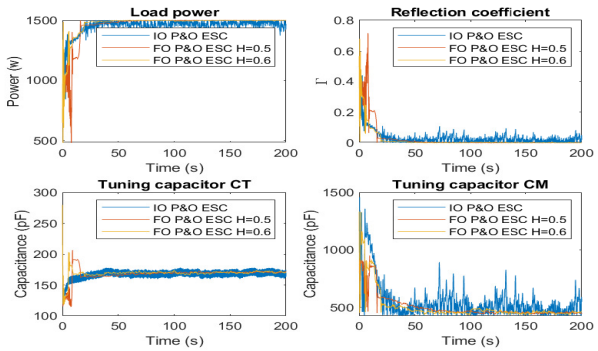

Fig. 9. P&O ESC and P&O FO-SESC controller with load $10-j10$ and IC=[50,50]

the convergence rate and settling time can reach reasonable values when $0.5 < H < 0.6$, and $0.5 < H < 0.6$ respectively. Thus, we can say that using dithering noises between $0.5 \leq H \leq 0.6$ the convergence rate of the ESC controller can be improved.

B. Test 2: P&O ESC and FO-SESC Controllers Global Convergence Analysis

This test analyzes the convergence rate, time, and reflected power RMS among the matching region of the L-Type network presented in Fig. 5. For the ESC controllers assessment, an extended set of capacitor initial conditions are defined, which corresponds to $IC = [0, 0], [10, 20], [35, 40], [50, 50], [100, 100]$ and each load is tested for different Hurst exponents $H = 0.1 : 0.1 : 0.9$. As an example, Fig. 12 shows the comparison of the P&O ESC controller matching zone regarding to the evolution of the P&O FO-SESC controller under the initial condition $IC = [0, 0]$ for $H = 0.1 : 0.1 : 0.9$. As can be observed, the P&O ESC controller convergence region contains 151 positive events. Besides, the P&O FO-SESC controller exhibit a variation of its convergence region according to the dithering noise Hurst exponent. If $H < 0.3$ or $H > 0.8$ the convergence region is significantly small compared with the P&O ESC controller. However, for $0.5 \leq H \leq 0.7$ the convergence region shows an increasing behavior, reaching

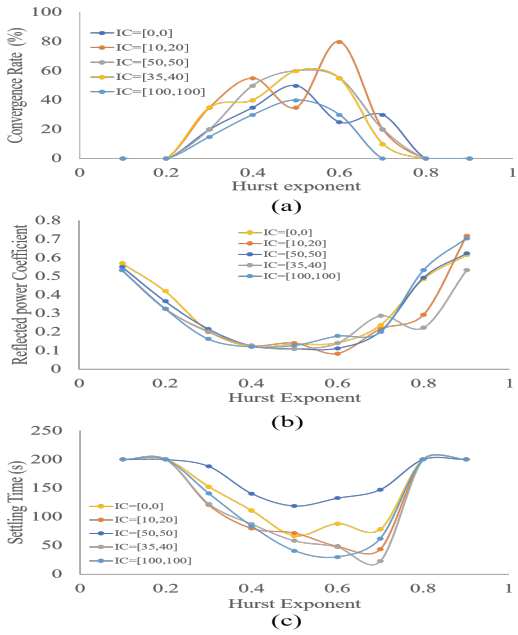

Fig. 10. Test 1: P&O FO-SESC controller average reflected power RMS vs Hurst exponent

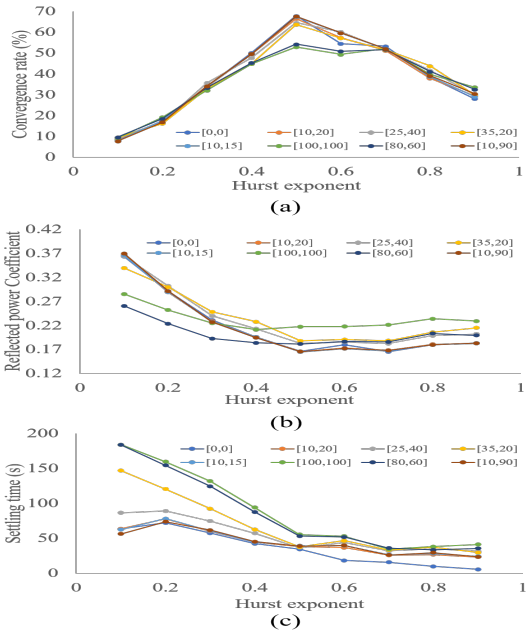

Fig. 11. (a) Average convergence rate, (b) reflected power RMS, and (c) settling time vs Hurst exponent on Test 2 for the overall matching region

its maximum at $H = 0.7$ with 171 positive convergence events.

Test 2 is repeated 10 times to analyze the average behavior of the P&O FO-SESC controller. The average convergence rate, settling time, and reflection power coefficient for the 10 tests against its Hurst exponent is shown in Fig. 11. As can be observed, the convergence rate in Fig. 11a of the P&O FO-SESC controller increases above 60% when $0.5 <= H < 0.6$, with a minimum convergence rate at $H < 0.1$. On the other hand, the reflected power RMS and settling time in Fig. 11b and Fig. 11c shows a decreasing behavior as the Hurst exponent increases; however, the convergence rate for $H > 0.6$ suffers a significant decrease, introducing a trade-off between convergence rate, settling time, and reflected power. Thus, we can say that the best operation range for the P&O FO-SESC controller can be reached for $0.5 \leq H \leq 0.6$ in the presence of different loads.

C. Test 3: ESC Controllers Capacitor Initial Condition Robustness Analysis

In this test, the ESC controller convergence is evaluated in terms of the capacitor initial condition space. Thus, a set of 25 different loads inside the matching space are evaluated against 25 IC in the range $C_t = 0 : 25 : 100$ and $C_m = 0 : 25 : 100$. Fig. 13 shows the initial condition capacitor space evolution using the P&O ESC and the P&O FO-SESC controllers for the load $Z_l = 15 - j25\Omega$. As can be observed, increasing the Hurst exponent can improve the convergence rate of the impedance matching. After repeating this test 10 times, the global average convergence rate of the P&O FO-SESC controller is shown in Fig. 14. As can be observed, the convergence rate can be increased up to 80% with $0.5 \leq H \leq 0.6$. Likewise, this behavior is consistent with

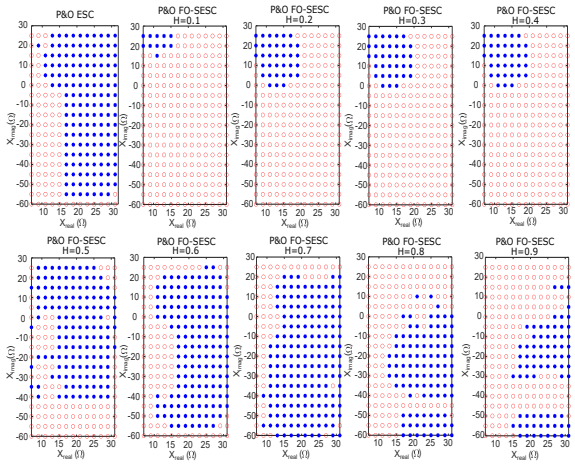

Fig. 12. Test 2: P&O FO-SESC controller convergence region evolution against Hurst exponent (blue is success, red is unsuccessful)

the obtained results from Tests 1 and 2. Therefore, we can say that using fractional-order dithering noise it is possible to improve the global performance of plasma impedance matching without feedforward or additional compensation mechanisms in the presence of variable load inside the matching and capacitor spaces.

VI. Conclusions and Future Works

A Perturb and Observe Fractional-Order Stochastic Extremum Seeking Control (P&O FO-SESC) with dithering noise was designed for plasma impedance matching. A L-type network with two variable capacitors was employed to perform the matching control. The P&O FO-SESC controller was tested for single and multiple loads under different initial conditions and different levels of LRD on the dithering noise

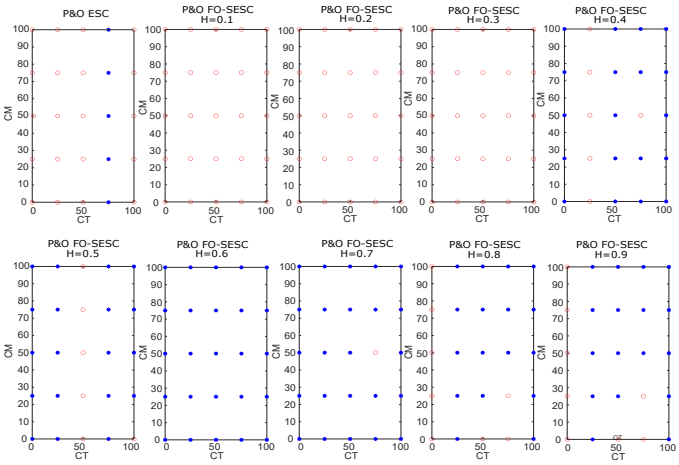

Fig. 13. Test 3: P&O FO-SESC controller capacitor initial conditions space vs Hurst exponent for $Z_l = 15 - j25\Omega$ (blue is success, red is unsuccessful)

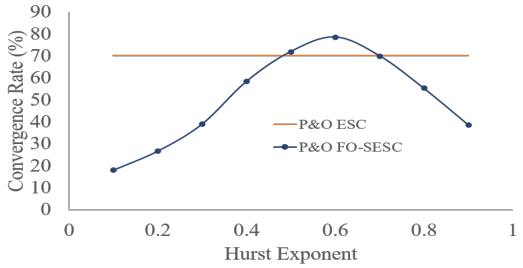

Fig. 14. Test 3: P&O ESC and P&O FO-SESC controller average Settling time vs Hurst exponent

given by the Hurst exponent. Obtained results show that using a dithering noise in the P&O FO-SESC controller in the range $0.5 \leq H \leq 0.6$ can improve the system convergence rate, settling time, and minimize the total reflected power during the impedance matching process. The P&O FO-SESC controller is robust under different loads and capacitor initial conditions, indicating that the P&O FO-SESC controller is suitable for plasma impedance matching where plasma load impedance is time variant and unknown.

As future works, the P&O FO-SESC controller design, simulation, and evaluation using the admittance model of the matching network instead of impedance is proposed based on Smith chart analysis. Likewise, introducing feedforward mechanisms based on magnitude and phase to improve ESC control performance can be considered.

REFERENCES

[1] Y. F. Li, "Analysis and design of tracking control for the RF matching box of plasma system," *ACM International Conference Proceeding Series*, pp. 18–23, 2019.

[2] S. Ishida, A. Kawamura, A. Takayanagi, and H. Takada, "Robust convergence of the impedance matching process based on seek control," *IECON Proceedings (Industrial Electronics Conference)*, pp. 1554–1559, 2011.

[3] Y. Ma and G. Wu, "Automatic impedance matching using simulated annealing particle swarm optimization algorithms for RF circuit," *Proceedings of 2015 IEEE Advanced Information Technology, Electronic and Automation Control Conference, IAEAC 2015*, pp. 581–584, 2016.

[4] Y. Hirose, A. Kawamura, A. Takayanagi, and H. Takada, "Analysis of impedance matching control," *2009 IEEE 6th International Power Electronics and Motion Control Conference, IPEMC '09*, vol. 3, pp. 1188–1191, 2009.

[5] C. Zhang and R. Ordóñez, *Extremum-Seeking Control and Applications*, 1st ed. London: Springer-Verlag London, 2012. [Online]. Available: http://link.springer.com/10.1007/978-1-4471-2224-1

[6] K. Bariyur and M. Krstic, *Real-time optimization by extremum-seeking control*. Wiley-Interscience, 2003.

[7] S.-J. Liu and M. Krstic, *Stochastic Averaging and Stochastic Extremum Seeking*. Springer, 2013, vol. 53, no. 9.

[8] C. Yin, Y. Chen, and S. M. Zhong, "Fractional-order sliding mode based extremum seeking control of a class of nonlinear systems," *Automatica*, vol. 50, no. 12, pp. 3173–3181, 2014. [Online]. Available: http://dx.doi.org/10.1016/j.automatica.2014.10.027

[9] S.-J. Liu and M. Krstic, "Stochastic Averaging in Continuous Time and Its Applications to Extremum Seeking," *IEEE Transactions on Automatic Control*, vol. 55, no. 10, pp. 2235–2250, 2010.

[10] D. Hollenbeck and Y. Chen, "A more optimal stochastic extremum seeking control using fractional dithering for a class of smooth convex functions," in *2020 IFAC World Congress*, 2020, pp. 1–6.

[11] P. Dix, B. Ashrafi, S. Drakunov, and U. Özguner, "ABS Control Using Optimum Search via Sliding Modes," *IEEE Transactions on Control Systems Technology*, vol. 3, no. 1, pp. 79–85, 1995.

[12] G. A. Frantsuzova, "Use of a Relay Controller for Automatic Extremum Seeking in Nonlinear Systems," *Avtometriya*, vol. 47, no. 3, pp. 274–280, 2011.

[13] R. L. Magin, "Fractional calculus in bioengineering." *Critical reviews in biomedical engineering*, vol. 32, no. 1, pp. 1–104, 2004.

[14] H. Sheng, Y. Chen, and T. Qiu, *Fractional Processes and Fractional-Order Signal Processing Techniques and Applications*. Springer, 2012.